JOURNAL OF DENTISTRY 40 (2012) 1074–1080

Available online at www.sciencedirect.com

SciVerse ScienceDirect

journal homepage: www.intl.elsevierhealth.com/journals/jden

Disruption of enamel crystal formation quantified by synchrotron microdiffraction

Maisoon Al-Jawad [a,*], Owen Addison [b], Malik Arshman Khan [a], Alison James [c], Christian J. Hendriksz [d]

[a] Queen Mary University London, Barts and the London School of Medicine and Dentistry, Institute of Dentistry, London E1 4NS, UK
[b] University of Birmingham, School of Dentistry, Birmingham B4 6NN, UK
[c] Birmingham Children's Hospital NHS Foundation Trust, Birmingham, B4 6NH, UK
[d] Salford Royal NHS Foundation Trust, Department of Adult Inherited Metabolic Diseases, Stott Lane, Salford, Greater Manchester, M6 8HD, UK

ARTICLE INFO

Article history:
Received 25 May 2012
Received in revised form
29 August 2012
Accepted 30 August 2012

Keywords:
Dental enamel
Biomineralization
Texture
Synchrotron microdiffraction
Crystallite orientation
Mucopolysaccharidosis

ABSTRACT

Objectives: To understand the pathology of the ultrastructure of enamel affected by systemic disorders which disrupt enamel tissue formation in order to give insight into the precise mechanisms of matrix-mediated biomineralization in dental enamel in health and disease.
Methods: Two-dimensional synchrotron X-ray diffraction has been utilized as a sophisticated and useful technique to spatially quantify preferred orientation in mineralized healthy deciduous dental enamel, and the disrupted crystallite organization in enamel affected by a systemic disease affecting bone and dental mineralization (mucopolysaccharidosis Type IVA and Type II are used as examples). The lattice spacing of the hydroxyapatite phase, the crystallite size and aspect ratio, and the quantified preferred orientation of crystallites across whole intact tooth sections, have been determined using synchrotron microdiffraction.
Results: Significant differences in mineral crystallite orientation distribution of affected enamel have been observed compared to healthy mineralized tissue. The gradation of enamel crystal orientation seen in healthy tissue is absent in the affected enamel, indicating a continual disruption in the crystallite alignment during mineral formation.
Conclusions: This state of the art technique has the potential to provide a unique insight into the mechanisms leading to deranged enamel formation in a wide range of disease states.
Clinical relevance: Characterising crystal orientation patterns and geometry in health and tanding of d to inform the appropriate dental management of these tissues and/or to investigate the influence of therapeutic interventions or external stressors which may impact on amelogenesis.

1. Introduction

Diseases associated with mineralization defects are frequently investigated using structural characterisation of affected hard tissues to complement an existing understanding of disease pathogenesis informed by cellular and molecular studies. A wide variety of techniques used to study bone and dental hard tissues include light and electron microscopy[1];

* *Corresponding author*. Tel.: +44 0 20 7882 5960.
E-mail address: m.al-jawad@qmul.ac.uk (M. Al-Jawad).
0300-5712
http://dx.doi.org/10.1016/j.jdent.2012.08.020

atomic force microscopy[2,3]; X-ray microtomography[4,5]; X-ray diffractometry[6–8]; and increasingly synchrotron X-ray scattering.[9–11] In particular electron microscopy studies can show qualitatively hierarchical features on the microscopic length-scale such as prismatic and interprismatic structures of enamel revealing the variation in prismatic structure between species showing that enamel ultrastructure and function are closely linked to evolutionary development.[12] In particular, recent evaluation of Hunter–Schreger bands in human enamel reveal that these specific prismatic orientations have evolved to optimise resistance to fracture and wear over the lifetime of an individual.[13,14]

Uniquely, synchrotron X-ray microdiffraction can determine spatial distributions of basic crystallographic parameters of the hydroxyapatite (HA) phase within mineralized tissues. Characterising crystal orientation patterns and geometry in health and following disruption can therefore become a powerful tool advancing our overall understanding of mechanisms leading to phenotypic expression. Dental hard tissues are unique in terms of their accessibility for such analyses. Deciduous teeth exfoliate naturally and permanent teeth are frequently available following routine extraction. More importantly dental enamel is highly mineralized and it's unique hierarchical structure forms incrementally over extended time periods with individual teeth mineralizing in 4–5 years. Accordingly disruption in crystallographic features of dental enamel due to disease progression or therapeutic intervention can be closely correlated with event time points.

The spectrum metabolic disorders known as mucopolysaccharidosis (MPS) diseases have incidences reported to range from 1:50,000 to 1:250,000 births[15] and will be used as a case study to highlight the capabilities of the technique. In particular mucopolysaccharidosis Type IVA (MPS IVA), or Morquio Syndrome, has manifestations in primary and secondary dentition. MPS IVA, an autosomal recessive lysosomal storage disease,[16,17] is characterised by reduced activity of enzyme N-acetylgalactosamine 6-sulphatase (GALNS) encoded by a gene on human chromosome 16q24.3[18,19] which leads to intracellular accumulation of partially degraded glycosaminoglycans (GAGs) keratan sulphate and chondroitin 6-sulphate in connective tissue, the skeletal system and teeth.[20,21] Clinically it manifests after infancy and is associated with severe skeletal abnormalities, restrictive lung disease, impaired endurance, hearing impairment, and aortic valvular disease.[22] Enzyme therapies developed for MPS IVA are currently being investigated through clinical trials (NCT ID: NCT01242111 and NCT01275066), with the potential to revolutionise treatment for patients.

Basic dental histological investigations have demonstrated that MPS IVA enamel is abnormally thin and pitted[23] with increased porosity correlating to the striae of Retzius.[24] Electron microscopy has revealed an interstitial layer of amorphous material 3–4 μm thick at the amelodentinal junction (ADJ).[25] In MPS IVA it has been suggested that pathological accumulation of GAGs occurs in the lysosomes of secretory stage ameloblasts.[21] However, there is no consensus on whether the effects of impaired lysosomal pathway function result in disturbances in protein secretion; matrix mineralization; degradation processes of amelogenins; or a combination which lead to the enamel structural changes. 2D synchrotron X-ray diffraction across whole intact sections of dental enamel can provide important insights into the spatial distribution of HA crystallite orientation.[9,26] The aim of this study was to ally detailed analysis of physical characteristics of affected enamel in a system with a known, precise, underlying genetic lesion. We aim to demonstrate that the technique can not only give novel insight into the mechanistic understanding of the disease pathogenesis (in MPS), but also provide better understanding of basic processes of enamel biomineralization in health by relating known genetic defects to measured changes in crystallographic parameters.

2. Materials and methods

2.1. Specimen preparation

Tooth specimens were collected following ethical approval (UK National Research Ethics Service Reference 08/H1202/119) and consent at Birmingham Children's Hospital NHS Foundation Trust. Two deciduous maxillary incisors from different patients affected by MPS IVA; one affected by MPS II (with no previous reported effect on enamel formation); and one healthy control deciduous maxillary incisor were used. Each extracted tooth, stored in thymol-saline solution, was serially sectioned bucco-lingually using a 0.3 mm diamond blade cutter (Met Prep, Coventry, United Kingdom) then polished to 100 μm thick. A spatially equivalent 0.4 mm × 0.2 mm area, located 1 mm superior to the enamel–cementum junction was identified as a representative and comparable region of interest on each tooth section. An illustration highlighting the equivalent region of interest on each tooth section is given in Fig. 1. For synchrotron studies tooth sections were kept hydrated during measurement using a reservoir of thymol-saline solution. For scanning electron microscopy the sections were dehydrated in ethanol, etched with 35% orthophosphoric acid for 15 s, and stored in a desiccator prior to use.

2.2. Experimental procedure

Synchrotron X-ray diffraction was used to explore the texture (or preferred orientation) of enamel crystallites in intact tooth sections. Preferred orientation refers to the degree of crystallite alignment. For a polycrystalline, isotropic material, there is random orientation of crystallites averaging the Bragg scattering intensity uniformly around the Debye rings of 2D X-ray diffraction patterns. However, a high degree of crystalline anisotropy, such as in dental enamel, produces a change in intensity around the Debye ring of Bragg reflections in two-dimensions correlating to the degree of crystallite alignment or ordering (Fig. 2, inset A). This change in intensity around Debye rings from different regions of enamel was measured to quantify the spatial texture distribution, and therefore the enamel crystallite organisation as a function of position.

2D synchrotron X-ray diffraction experiments were carried out on the XMaS beamline (BM28) at the European Synchrotron Radiation Facility (ESRF). Performing experiments at central synchrotron radiation facilities through a peer-reviewed beamtime application process, means there are

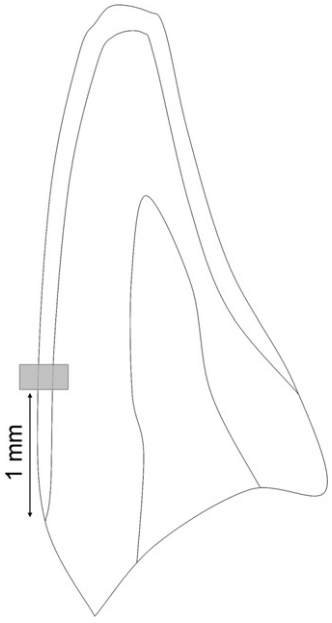

Fig. 1 – Illustration representing a typical section of deciduous incisor studied. The boxed region indicates the equivalence of the area of interest which was measured for each specimen.

strict time constraints such that carrying out repeatability studies is not straight forward. For this study (the first of its kind to explore texture variation in MPS affected tissue) it was decided to prioritise the collection of high quality, high resolution images instead of sampling many repeated specimens. Therefore the X-ray beamspot was defined as $20 \times 20\ \mu m$ using vacuum tube slits, and diffraction images were collected every 20 s. An X-ray energy of 15.0 keV was used – corresponding to a wavelength of 0.82 Å. Each specimen was mounted onto a goniometer on an XY-motorized travelling sample platform and aligned to the centre of rotation. A co-ordinate system for the region of interest on the tooth was established using a calibrated telescope. 2D X-ray diffraction images were collected using a 2048×2048 pixel CCD camera mounted perpendicular to the X-ray beam 170 mm from the sample. 2D maps were collected by translating the specimen relative to the beam in horizontal and vertical directions. Subsequently, scanning electron microscopy was used to image the same regions of interest on the enamel.

2.3. *Data analysis*

A total of eight hundred 2D diffraction images of enamel were processed with the Fit2d software.[27] Intensity patterns around the Debye ring of the (0 0 2) Bragg reflection were used to quantify the texture parameter (or preferred orientation) since this reflection is normal to the c-axis of enamel HA crystallites. The intensity was integrated over 360° in a narrow band containing the (0 0 2) reflection and plotted *versus* the azimuthal angle. The peaks were fitted to a Gaussian peak-shape and the full width half maximum (FWHM) value determined. By applying this procedure to each of the diffraction images, a spatial map of texture distribution in the (0 0 2) direction in the enamel was constructed.

The diffraction data of ten patterns close to the surface of the healthy enamel, and MPS IVA affected enamel respectively were summed and analysed by Rietveld refinement[28] using GSAS software.[29] The instrument parameters were calibrated using a LaB_6 standard sample. The two summed patterns were fitted with a HA phase with hexagonal space group $P6_3/m$. Lattice parameters, Lorentzian line broadening and spherical harmonic texture parameters were refined. Microstrain, although a refinable parameter within GSAS, was found to be negligible in these enamel specimens therefore was kept fixed.

3. Results

A typical diffraction pattern fitted to the calculated HA phase using Rietveld refinement is demonstrated in Fig. 2 together

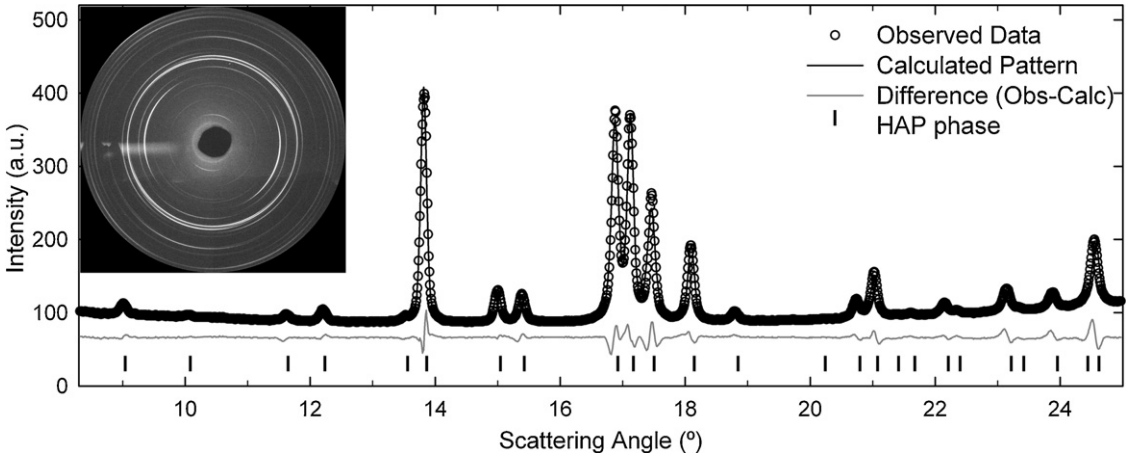

Fig. 2 – 1D diffraction pattern of healthy deciduous surface enamel with Rietveld refinement including the observed data (open circles), the calculated diffraction pattern (black solid line), the difference curve (grey solid line) and the tick marks for the 2θ peak positions for the calculated diffraction pattern of HA. The inset shows the summed 2D X-ray image for this pattern.

Table 1 – Refined structural parameters for surface enamel diffraction patterns fitted with HA phase. The low χ^2 value (<1.0) is likely due to low-noise summed area detector data which has been converted into 1D underestimating the collection statistics.

Parameter	Healthy enamel	MPS IVA affected enamel
Space group	$P6_3/m$	$P6_3/m$
a (Å)	9.2514(3)	9.2655(3)
c (Å)	6.7347(2)	6.7402(2)
$p_{\|\|}$ (nm)	109.16(7)	86.7(6)
$p_{\perp}$ (nm)	43.86(3)	49.84(3)
$p_{\|\|}/p_{\perp}$	2.49(3)	1.74(2)
$0\,0\,2_{(SH)}$	5.6(1)	4.9(1)
χ^2	0.4	0.2

with its 2D X-ray diffraction image (Fig. 2. inset). The tabled results of the refinement are given in Table 1. Lattice parameters (a and c), Lorentzian line broadening ($p_{||}$ and $p_{\perp}$), and spherical harmonic texture parameters ($0\,0\,2_{(SH)}$) were refined producing a good fit to the HA phase. Lorentzian line broadening was refined to find the anisotropic particle sizes from the Scherrer equation. The parallel ($p_{||}$) and perpendicular ($p_{\perp}$) components to the anisotropic particle size effects were given by:

$$p_{\|} = \frac{1620\lambda}{\pi(X + X_e)} \text{ and } p_{\perp} = \frac{1620\lambda}{\pi X}$$

where λ is the X-ray wavelength; X is Lorentzian particle size broadening; and X_e is the anisotropic coefficient of Lorentzian broadening.[29]

An example of the typical variations in Intensity around the (0 0 2) Debye ring for healthy and MPS IVA affected enamel are plotted in Fig. 3 with a Gaussian peak shape fitted to determine the FWHM. It was observed that the FWHM of affected enamel is over double that of healthy enamel, indicating less orientation of crystallites in affected enamel.

The results of the texture distribution analysis are shown in Fig. 4a–d. The x-axis represents distance from the surface enamel towards the ADJ and the y-axis represents vertical distance. In healthy enamel (Fig. 4a) the FWHM values decrease as a function of distance from the enamel surface. In contrast the FWHM values of the MPS II and MPS IVA affected enamel (Fig. 4b–d) do not vary significantly as a function of distance.

Fig. 5 shows four typical scanning electron micrographs for the healthy deciduous enamel section (Fig. 5a–d), and for MPS IVA affected enamel (Fig. 5e–h). In Fig. 5d (healthy enamel close to ADJ) clear scalloping (Fig. 5d, arrow 1) and close integration of dentine and enamel can be seen with a small region of closely packed enamel crystallites at the ADJ (Fig. 5d, arrow 2), with prismatic order emerging ~5 μm from the ADJ. In contrast in Fig. 5h (MPS IVA affected enamel close to ADJ) there is no evidence of scalloping, instead a microgap between dentine and enamel is observed (Fig. 5h, arrow 3). Compared to the healthy ADJ, there is a larger region of tightly packed enamel crystallites (Fig. 5h, arrow 4), and a less well defined prismatic order emerges. In the healthy enamel closer to the surface (Fig. 5a–c) there is good differentiation between prisms and interprismatic enamel (Fig. 5c, arrow 5); sharp, well defined crystallite boundaries; and a uniform prismatic structure. Whereas in the MPS IVA affected enamel (Fig. 5e–g) a non-uniform prismatic structure emerges with atypical prism shapes (Fig. 5f, arrow 6); larger regions of aprismatic enamel; and the individual crystallites are less well defined.

4. Discussion

There is a 0.2% variation in lattice parameter between healthy and affected enamel. Enamel is not pure hydroxyapatite, rather a carbonate substitute apatite, with CO_3^{2-} concentrations ranging from 1–5% from surface to tissue interior.[30] The 0.2% variation lies within the intratooth variations we have reported previously of 0.1–0.6%[9] therefore is likely to be attributed to slight variations in chemical composition rather than related to the metabolic disorder.

The anisotropic particle size broadening varies between healthy and MPS IVA affected enamel, with the crystallite

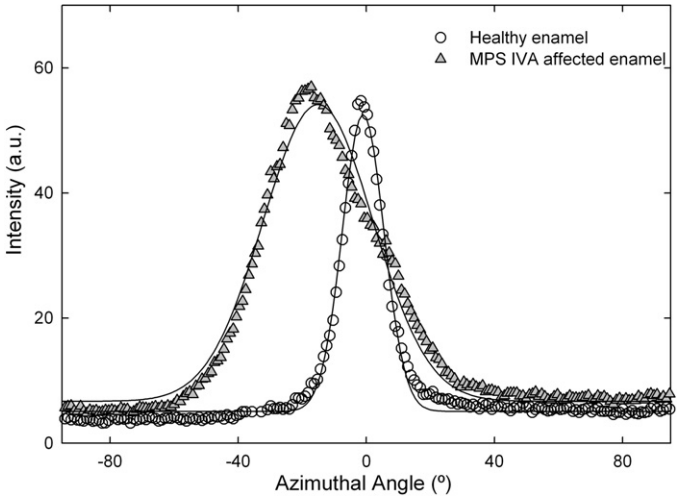

Fig. 3 – The variation in intensity around the Debye ring of the (0 0 2) Bragg reflection close to the surface of the healthy enamel (open circles), and close to the surface of MPS IVA affected enamel (solid triangles). The error bars lie within the data points. The solid line is a fit to a Gaussian peak shape from which the FWHM values were determined.

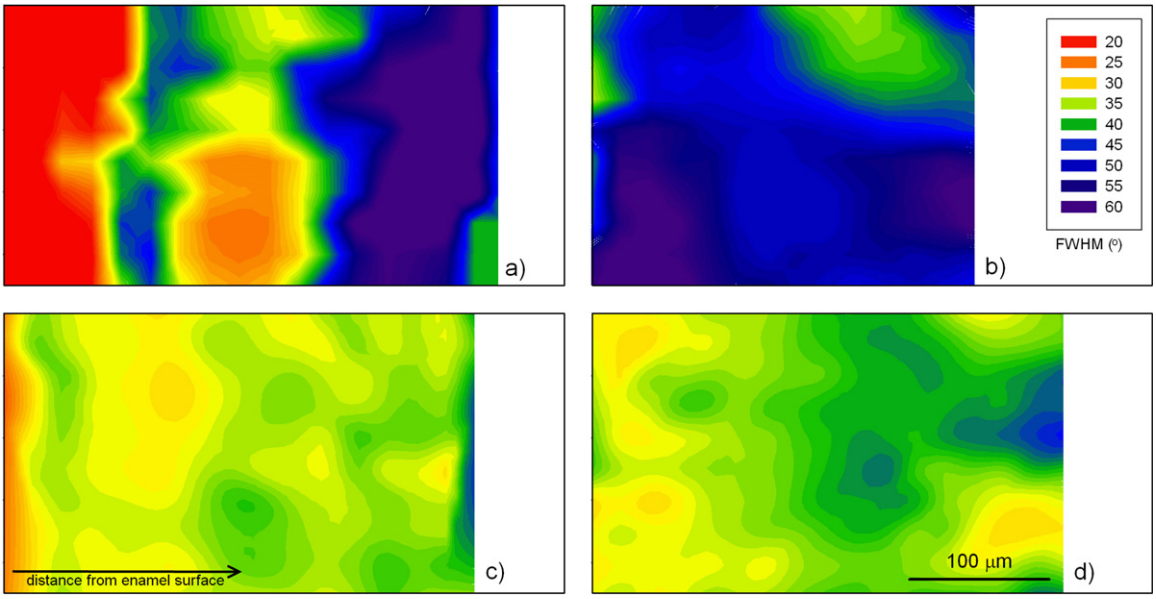

Fig. 4 – Texture distribution maps showing the degree of crystallite alignment in (a) healthy deciduous incisor, (b) deciduous incisor affected by MPS II, (c) and (d) deciduous incisor affected by MPS IVA. The *x*-axis represents distance from the surface enamel (left-hand side) towards the ADJ (right-hand side) and the *y*-axis represents vertical distance at the same scale. The colour scale is the FWHM (in degrees) of the azimuthal peaks fitted to a Gaussian peak-shape.

aspect ratio ($p_{\parallel}/p_{\perp}$) 2.49(3) for healthy enamel and 1.74(2) for the MPS IVA affected enamel. This indicates that for surface enamel the HA crystallites are smaller and less anisotropic in MPS IVA enamel as compared to healthy enamel. This correlates with the statistically significant higher texture parameter ($0\,0\,2_{(SH)}$) of 5.6(1) for healthy enamel as compared to that of MPS IVA enamel 4.9(1).

Results presented in Fig. 4 indicate that texture distributions in MPS II and IVA enamel are substantially different to that of healthy enamel. In healthy deciduous enamel (Fig. 4a) there is a steady decrease in ordering (crystallite alignment) as a function of depth into the tooth. We have reported a similar trend in the past in the permanent dentition, where we observed that HA crystallites are most aligned in the cuspal

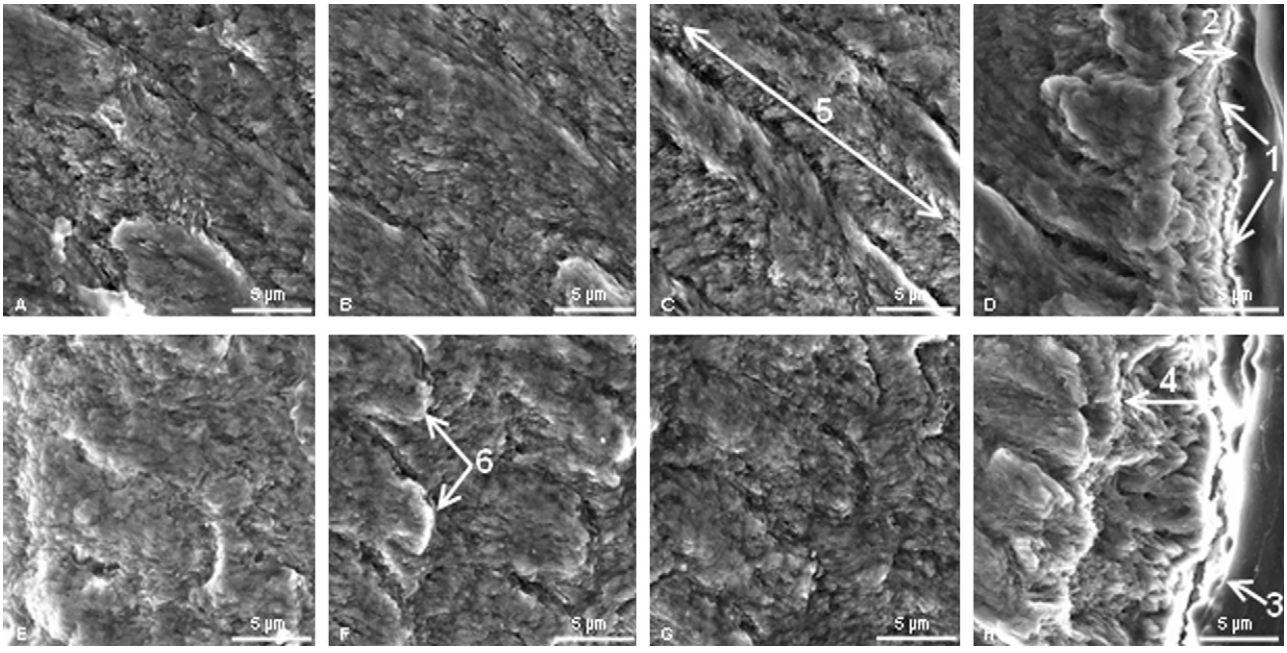

Fig. 5 – Scanning electron micrographs taken from the surface towards the ADJ going from left to right for (a)–(d) Healthy deciduous enamel and (e)–(h) enamel affected by MPS IVA. Features are highlighted with arrows: scalloping (1), close crystallite packing (2 and 4), microgap (3), prism/interprism boundary (5), non-uniform prism structure (6). The magnification is the same for each image and the scale bar is given.

regions, whilst along sides of the tooth away from the cusps and deeper into the enamel, crystallites are less ordered, likely due to the convolution of prism directions which occurs towards the ADJ.[9,26] In contrast, the plots shown in Fig. 4b–d indicate that the texture in MPS II and IVA affected enamel does not vary as a function of depth into the enamel. Instead the degree of crystallite ordering remains constant throughout the tooth thickness. This trend is seen also on the prismatic length scale from the SEM images shown in Fig. 5.

In MPS IVA the deficiency of N-acetylgalactosamine 6-sulphatase (GALNS) manifests clinically and radiographically in enamel which is hypoplastic and can detach easily from the underlying dentine. Generally a thin enamel layer is indicative of a developmental disturbance during the secretory stage of amelogenesis. Through *in situ* hybridization of a day 1 mouse incisor it has been shown that GALNS mRNA is most abundant in secretory ameloblasts.[21] Therefore it is likely that the disruption in the texture gradation and reduced ordering in the prismatic structure we observed in MPS IVA affected enamel is likely to start in the secretory stage of amelogenesis. However, although mineralization starts in the secretory stage, the thickening of enamel crystallites, where the degree of preferred orientation is defined continues through the maturation stage, therefore it is likely that the texture distribution is determined by disruption of cellular and matrix-mediated events at both stages. At the earliest stages of amelogenesis, it has been suggested that GAGs may serve as a matrix for anchoring amelogenin at the ADJ so that a close bond is established between enamel and dentine.[31] The absence of good integration between enamel and dentine at the ADJ of the MPS IVA enamel (Fig. 5h) may be indicative of the lack of the specific sulphatase which should remove the GAGs from the dentine tubule sites to allow proper intergration at the ADJ.

In addition, normal enamel matrix mineralization has been demonstrated to be disrupted in animal models by suppression of Ca^{2+}ATPase activity and ATP-dependent calcium pumps are observed ultracytochemically at specific regions of the Tomes process of ameloblasts.[32] Moreover, the potential role of Ca^{2+} trafficking has been reported in many lysosomal storage disorders including evidence for a potential link with mitochondrial dysfunction.[33] This was not predicted to be present in patients affected by MPS IVA but these findings in enamel may provide some evidence that other tissues like bone and muscle should be investigated in this cohort.

To the authors' knowledge there have been no reports of enamel defects associated with Hunter syndrome (MPS II), however in this study we clearly see disturbances in MPS II enamel crystal organisation. In fact, disruption in enamel texture appears more severe in MPS II than in MPS IVA. Accumulation of GAGs in the dental follicle of developing teeth in other MPS diseases, such as Hurler syndrome (MPS I) has been reported in the past,[23] but dental abnormalities are not always clinically obvious. It may be in MPS II the disruption affects the crystallography and nanostructure of enamel but has not yet been detected clinically on the macroscale.

We have shown that the use of 2D synchrotron microdiffraction, a state of the art technique, has the potential to provide unique insights into the mechanisms leading to deranged enamel formation in a disease state. The detailed characterisation of apatite crystallite orientation in dental enamel can provide an accessible and minimally invasive route to improve our understanding of the biomineralization process in enamel and our understanding of pathogenesis of systemic disturbances affecting mineralization. The structural information provided may have direct relevance for clinicians managing disease prevention or restoration of these tissues. For example, in the scenario provided, the lack of regular HA crystal orientation throughout the enamel thickness in MPS II and IVA may explain the poor success of adhesive restorations bonded to etched-enamel which is observed clinically.[15]

5. Conclusions

We have used 2D synchrotron X-ray diffraction to study the texture distribution in enamel affected by MPS IVA and II. Significant differences were observed in the texture distribution of the MPS IVA and II affected enamel as compared to healthy tissue, characterised by less gradation of enamel crystal orientation in MPS-affected enamel compared to healthy tissue. The use of this state of the art technique has the potential to provide a unique insight into the mechanisms leading to deranged enamel formation in a wide range of disease states.

Acknowledgements

This work was performed on the EPSRC-funded XMaS beamline at the ESRF, directed by M.J. Cooper, C.A. Lucas and T.P.A. Hase. We are grateful to the beamline team of S.D. Brown, O. Bikondoa, D. Wermeille, L. Bouchenoire and P. Thompson for their invaluable assistance, and to S. Beaufoy and J. Kervin for additional support.

REFERENCES

1. Landis WJ, Song MJ, Leith A, McEwen L, McEwen BF. Mineral and organic matrix interaction in normally calcifying tendon visualized in 3 dimensions by high-voltage electron-microscopic tomography and graphic image-reconstruction. *Journal of Structural Biology* 1993;**110**:39–54.
2. Marshall GW, Marshall SJ, Kinney JH, Balooch M. The dentin substrate: structure and properties related to bonding. *Journal of Dentistry* 1997;**25**:441–58.
3. Kirkham J, Zhang J, Brookes SJ, Shore RC, Wood SR, Smith DA, *et al.* Evidence for charge domains on developing enamel crystal surfaces. *Journal of Dental Research* 2000;**79**:1943–7.
4. Davis GR, Wong FSL. X-ray microtomography of bones and teeth. *Physiological Measurement* 1996;**17**:121–46.
5. Huang TTY, Jones AS, He LH, Darendeliler MA, Swain MV. Characterisation of enamel white spot lesions using X-ray micro-tomography. *Journal of Dentistry* 2007;**35**:737–43.
6. Young RA, Mackie PE. Crystallography of human tooth enamel: initial structure refinement. *Materials Research Bulletin* 1980;**15**:17–29.
7. Hirota F. Prism arrangement in human cusp enamel deduced by X-ray diffraction. *Archives of Oral Biology* 1982;**27**:931–7.

8. Almer JD, Stock SR. Internal strains and stresses measured in cortical bone via high-energy X-ray diffraction. *Journal of Structural Biology* 2005;**152**:14–27.
9. Al-Jawad M, Steuwer A, Kilcoyne SH, Shore RC, Cywinski R, Wood DJ. 2D mapping of texture and lattice parameters of dental enamel. *Biomaterials* 2007;**28**:2908–14.
10. Kinney JH, Pople JA, Driessen CKH, Breunig TM, Marshall GW, Marshall SJ. Intrafibrillar mineral may be absent in dentinogenesis imperfecta type II (DI-II). *Journal of Dental Research* 2001;**80**:1555–9.
11. Stock SR, Veis A, Telser A, Cai Z. Near tubule and intertubular bovine dentin mapped at the 250 nm level. *Journal of Structural Biology* 2011;**176**:203–11.
12. Maas MC, Dumont ER. Built to last: the structure, function, and evolution of primate dental enamel. *Evolutionary Anthropology* 1999;**8**:133–52.
13. Lynch CD, O'Sullivan VR, Dockery P, McGillycuddy CT, Sloan AJ. Hunter-Schreger Band patterns in human tooth enamel. *Journal of Anatomy* 2010;**217**:106–15.
14. Lynch CD, O'Sullivan VR, McGillycuddy CT, Dockery P, Rees JS, Sloan AJ. Hunter-Schreger Bands and their implications for clinical dentistry. *Journal of Oral Rehabilitation* 2011;**38**:359–65.
15. James A, Hendriksz C, Addison O. The oral health needs of children, adolescents and young adults affected by a mucopolysaccharide (MPS) disorder. *Journal of Inherited Metabolic Disease Reports* 2012;**2**:51–8.
16. Northover H, Cowie RA, Wraith JE. Mucopolysaccharidosis type IVA (Morquio syndrome): a clinical review. *Journal of Inherited Metabolic Disease* 1996;**19**:357–65.
17. Nelson J, Crowhurst J, Carey B, Greed L. Incidence of the mucopolysaccharidoses in Western Australia. *American Journal of Medical Genetics A* 2003;**123**:310–3.
18. Baker E, Guo XH, Orsborn AM, Sutherland GR, Callen DF, Hopwood JJ, *et al.* The Morquio A syndrome (mucopolysaccharidosis IVA) gene maps to 16q24.3. *American Journal of Human Genetics* 1993;**52**:96–8.
19. Masuno M, Tomatsu S, Nakashima Y, Hori T, Fukuda S, Masue M, *et al.* Mucopolysaccharidosis IV A: Assignment of the human N-acetylgalactosamine-6-sulfate sulfatase (GALNS) gene to chromosome 16q24. *Genomics* 1993;**16**:777–8.
20. Hollister DW, Cohen AH, Rimoin DL, Silberberg R. Morquio syndrome (mucopolysaccharidosis 4) – morphologic and biochemical studies. *Johns Hopkins Medical Journal* 1975;**137**:176–83.
21. Yamakoshi Y, Hu JCC, Liu SX, Sun XL, Zhang CH, Oida S, *et al.* Porcine N-acetylgalactosamine 6-sulfatase (GALNS) cDNA sequence and expression in developing teeth. *Connective Tissue Research* 2002;**43**:167–75.
22. Hendriksz CJ, Al-Jawad M, Berger KI, Hawley SM, Lawrence R, McArdle C, et al. Clinical overview and treatment options for non-skeletal manifestations of mucopolysaccharidosis Type IVA. *Journal of Inherited Metabolic Disease*, http://dx.doi.org/10.1007/s10545-012-9459-0, in press [E-pub ahead of print].
23. Gardner DG. The oral manifestations of Hurler's syndrome. *Oral Surgery Oral Medicine Oral Pathology* 1971;**32**:46–57.
24. Rølling I, Clausen N, Nyvad B, Sindet-Pedersen S. Dental findings in three siblings with Morquio's syndrome. *International Journal of Paediatric Dentistry* 1999;**9**:219–24.
25. Lustmann J. Dentinoenamel junction area in primary teeth affected by Morquio's syndrome. *Journal of Dental Research* 1978;**57**:475–9.
26. Simmons LM, Al-Jawad M, Kilcoyne SH, Wood DJ. Distribution of enamel crystallite orientation through an entire tooth crown studied using synchrotron X-ray diffraction. *European Journal of Oral Sciences* 2011;**119**:19–24.
27. Hammersley AP. FIT2D: an introduction and overview. *ESRF Internal Report* 1994; ESRF97HA02T.
28. Rietveld HM. A profile refinement method for nuclear and magnetic structures. *Journal of Applied Crystallography* 1969;**2**:65–71.
29. Larson AC, Von Dreele RB. General structure analysis system (GSAS). *Los Alamos National Laboratory Report LAUR* 2004:86–748.
30. Weatherell JA, Robinson C, Hallsworth AS. Variations in chemical composition of human enamel. *Journal of Dental Research* 1974;**53**:180–92.
31. Ravindranath RMH, Basilrose SRM. Localization of sulfated sialic acids in the dentinal tubules during tooth formation in mice. *Acta histochemica* 2005;**107**:43–56.
32. Sasaki T, Takagi M, Yanagisawa T, Structure and function of secretory ameloblasts in enamel formation. In Chadwick DJ, Cardew G, editors. *Dental Enamel CIBA Foundation Symposium*, 205. Chichester: John Wiley & Sons Ltd; 1997. p. 32–53.
33. Pereira VG, Gazarini ML, Marcos L, Rodrigues LC, Da Silva FH, Han SW, *et al.* Evidence of lysosomal membrane permeabilization in mucopolysaccharidosis Type I: rupture of calcium and proton homeostasis. *Journal of Cellular Physiology* 2010;**223**:335–42.